INSTITUTE OF PHYSICS PUBLISHING JOURNAL OF PHYSICS D: APPLIED PHYSICS

J. Phys. D: Appl. Phys. **39** (2006) 4366–4376 doi:10.1088/0022-3727/39/20/012

LES modelling of an unconfined large-scale hydrogen–air deflagration*

Vladimir Molkov[1,3], **Dmitriy Makarov**[1] **and Helmut Schneider**[2]

[1] FireSERT Institute, University of Ulster, Newtownabbey, Co. Antrim BT37 0QB, UK
[2] Fraunhofer Institute on Chemical Technology, Joseph-von-Fraunhoferstr. 7, 76327 Pfinztal, Germany

E-mail: v.molkov@ulster.ac.uk

Received 16 February 2006, in final form 28 July 2006
Published 29 September 2006
Online at stacks.iop.org/JPhysD/39/4366

Abstract

This paper describes the large eddy simulation modelling of unconfined large-scale explosions. The simulations are compared with the largest hydrogen–air deflagration experiment in a 20 m diameter hemispherical polyethylene shell in the open. Two combustion sub-models, one developed on the basis of the renormalization group (RNG) theory and another derived from the fractal theory, were applied. Both sub-models include a sub-grid scale model of the turbulence generated by flame front itself based on Karlovitz's theory and the observation by Gostintsev *et al* on a critical distance for transition from laminar to self-similar flame propagation regime. The RNG sub-model employs Yakhot's formula for turbulent premixed flame propagation velocity. The best fit flame propagation dynamics is obtained for the fractal sub-model with a fractal dimension $D = 2.22$. The fractal sub-model reproduces the experimentally observed flame acceleration during the whole duration of explosion, accurately simulating the negative phase of the pressure wave but overestimating by 50% the positive phase amplitude. The RNG sub-model is closer to the experiment in predicting the positive phase but under-predicts by 30% the negative phase amplitude. Both sub-models simulate experimental flame propagation up to 20 m and pressure dynamics up to 80 m with reasonable accuracy.

(Some figures in this article are in colour only in the electronic version)

Nomenclature

A	Flame area, m^2
CFL	Courant–Friedrichs–Lewy number
C	Hydrogen concentration in a mixture, % by volume
c	Progress variable (normalised product mass fraction)
c_p	Specific heat capacity of mixture at constant pressure, $c_p = \sum_m c_{p_m} Y_m$
D	Fractal dimension
E	Total energy, $J\,kg^{-1}$ $E = h - p/\rho + u^2/2$
E_{act}	Activation energy, $J\,mol^{-1}$
E_i	Expansion coefficient, $E_i = \rho_u/\rho_b$
E_{ign}	Ignition energy, J
g	Gravitational acceleration, $m\,s^{-2}$
$H(x)$	Heaviside function
H_c	Heat of combustion, $J\,kg^{-1}$
h	Enthalpy, $J\,kg^{-1}$, $h = \int_{298.15}^{T} c_p\,dT$
M	Molecular mass, $kg\,kmole^{-1}$, $M = \sum_m V_m M_m$
m_0	Temperature index in dependence of burning velocity on temperature
n_0	Baric index in dependence of burning velocity on pressure
Pr	Prandtl number, $Pr = \mu c_p/k$, where k is thermal conductivity W/m/K
p	Pressure, Pa
R	Radius, m
R_0	Characteristic radius for onset of fractal, self-similar regime of the turbulent flame front propagation, m

* This paper was presented at the Second International Synposium on Nonequilibrium Processes, Combustion, and Atmospheric Phenomena (Dagomys, Sochi, Russia, 3–7 October 2005).

[3] Author to whom any correspondence should be addressed.

R_{sph}	Initial radius of the hydrogen–air cloud (radius of polyethylene balloon), m
R_{univ}	Universal gas constant, 8314.4 J K^{-1} kmol^{-1}
S_c	Source term in conservation equation for progress variable, kg m^{-3}s^{-1}
S_E	Source term in energy conservation equation, J m^{-3}s^{-1}, $S_E = S_c H_c$
$\tilde{S}_{ij}$	Rate of strain tensor, s^{-1}
Sc	Schmidt number, $Sc = \mu/\rho D$, where D is the diffusion coefficient, m^2 s^{-1}
S_t	Turbulent burning velocity, m s^{-1}
S_{u0}	Laminar burning velocity at initial conditions, m s^{-1}
S_u	Laminar burning velocity, m s^{-1}
T	Temperature, K
t	Time, s
$u_{i,j,k}$	Velocity components, m s^{-1}
u'	Root-mean square of SGS velocity component, m s^{-1}
V	Volume, m^3
$x_{i,j,k}$	Spatial coordinates, m
Y	Mass fraction

Greek

Δp_F	Peak overpressure associated with flame propagation through pressure transducer location, kPa
Δ_{CV}	Control volume characteristic size, m
Δt	Time step, s
λ_o	Outer cut-off of the fractal structure, m
λ_i	Inner cut-off of the fractal structure, m
ε	Overall thermokinetic index, $\varepsilon = m_0 + n_0 - m_0/\gamma_u$
γ	Specific heat ratio
μ	Dynamic viscosity, Pa s
ρ	Density, kg m^{-3}, $\rho = (pM)/(R_{univ}T)$
Ξ_{SGS}	SGS flame front wrinkling factor
Ξ_{MAX}	Maximum SGS flame front wrinkling factor due to turbulence generated by the flame front itself

Subscripts and superscripts

a	Air
b	Burned mixture
c	Source term in progress variable equation
E	Source term in energy conservation equation
eff	Effective value
f	Fuel
hsph	Hemispherical
H_2	Hydrogen
i, j, k	Spatial coordinate indexes
m	m-th component of gas mixture
MAX	Maximum
SGS	Sub-grid scale
Stoich	Stoichiometric
t	Turbulent
u	Unburned mixture
0	Initial conditions

Bars

$\bar{}$	LES filtered quantity
$\tilde{}$	LES mass-weighted filtered quantity

1. Introduction

The use of hydrogen as an energy carrier and its wide introduction into the market throughout the world, especially transportation and storage, raises many questions if compromising safety is to be avoided. Explosion of hydrogen–air mixtures in the open atmosphere is one of the likely scenarios. Analysis of unscheduled releases, followed by disastrous explosions, can be performed through examination of on-site blast data, infrasound and ionosphere effects and their numerical simulations. But first the physics of the process should be understood and computational fluid dynamics models need be developed and validated against large-scale experiments to provide predictive tools for hydrogen safety engineering. Ten years ago predictive modelling of turbulent deflagration was not possible [1]. In this paper we demonstrate the capability of the large eddy simulation (LES) model developed from the first principles to simulate dynamics of the largest unconfined hydrogen–air deflagration ever performed [2].

The emphasis in combustion research for energy applications differs from that in accidental combustion research, i.e. fire and explosion safety research. Significant flow turbulence, high flame strain rates and relatively small scales of inhomogeneous regions are characteristic for most combustion devices. These features can differ significantly from those in large-scale unwanted combustion. The initial flame propagation after accidental ignition usually takes place in a quiescent or moderately agitated mixture in a quasi-laminar mode. While the combustion community is mainly focused on the aspects of flame behaviour to increase the efficiency of combustion devices, explosion safety researchers are focused on combustion mitigation through a proper prediction of flow, pressure and temperature dynamics during unwanted flame propagation in complex geometries under various conditions, usually attributed to essentially larger scale experiments. Conventional models, used to design combustion devices, may not be appropriate to analyse large-scale explosions as the regularities and physical phenomena for freely propagating accidental flames are different from those for stabilized flames, e.g. burner flames. In particular larger scale and/or low stretch rate are typical for large-scale unconfined explosions [3].

LES technique is promising for deflagration simulation as it avoids time averaging and allows better prediction of highly non-isotropic turbulent flows and large-scale flame flow interaction at the resolved level [4, 5]. In most approaches to LES of premixed combustion there is a numerical requirement for a minimum number of computational grid points within the simulated flame front thickness, normally 4–5 points [4], independent of the mesh size. Unstructured grids are recommended for LES in complex geometries [6]. For tetrahedral unstructured grids 4–5 points through the numerical flame front thickness can be 'collected' at a distance equal to 2–3 edges of tetrahedral control volume (CV). It means that LES can resolve elements of a flame front structure with a size larger than about 4–6 edges of the tetrahedron of the applied mesh, and smaller sub-grid structures can be only modelled.

There are different views on the possibility of the deflagration to detonation transition (DDT) in fuel–air mixtures initiated by a weak source such as a spark. Literature

Table 1. Experimental conditions and results for different tests [2].

Test No.	C, % vol.	T_i, K	p_i, kPa	E_{ign}, J	V, m^3	Hemisphere diameter, m	Maximum flame speed, m s^{-1}
GHT 23	29.1	282	98.1	10	7.5	3.06	43
GHT 26	29.2	281	99.1	1000	7.5	3.06	43
GHT 39	29.4	279	98.5	1000	50	5.76	50
GHT 40[a]	29.5	279	98.5	150	50	5.76	54
GHT 11	31.0	281	100.7	314	262	10.0	60
GHT 13	25.9	283	100.9	314	262	10.0	48
GHT 34[a]	29.7	283	98.9	150	2094	20.0	84

[a] Experiments with rhombus-shaped wire net over the hemispherical balloon.

review [7] indicates that there is no reliable data on DDT in unconfined clouds of combustible gases. Theoretical considerations [8] admit DDT of free spherical premixed combustion due to flame front instabilities and acceleration. Hydrogen–air deflagrations in unconfined conditions (rubber balloons) were studied experimentally in Russia in 1983 [9]. A spark with energy of 1 J was used to ignite a mixture in the centre of a balloon with a volume of 35 or 86 m^3 (diameter about 4 m and 5.5 m, respectively). Experiments in a 4 m diameter balloon demonstrated that flame front acceleration at the initial stage of combustion ceased and the flame propagated with a practically constant velocity of 38 m s^{-1} (35% by volume of hydrogen). In a 5.5 m diameter balloon test the flame propagation velocity was continuously increasing to 105 m s^{-1} for the mixture with the same concentration of hydrogen. The authors [9] concluded that the maximum velocity is increasing with diameter of an initial cloud, and for volume larger than 500 m^3 (diameter larger than 10 m), DDT is possible. In the same year experimental studies with hemispherical volumes of up to 2094 m^3 were performed in Germany [2, 10, 11]. Tests were conducted with ignition sources of energy within the range from 10 to 1000 J in near stoichiometric hydrogen–air clouds with diameter of hemisphere up to 20 m, but no DDT was registered.

The characteristics of blast waves, from unconfined deflagrations, are determined by gaseous cloud combustion and differ from that of high explosives. For example, in the near-field the overpressure from the positive phase of gaseous explosion is much less compared with that from high explosives, while the duration of the phase is greater. In the far-field, pressure waves from deflagrations decay more slowly with distance from a source of initiation and cannot be described by means of the TNT-equivalence concept [12, 13]. The TNT-equivalence concept is inadequate to describe the large amplitude of the negative phase of gaseous explosions [13], which is larger than the positive phase amplitude for deflagrations [12].

In 1999 Bradley suggested that in the case of large-scale explosion flames 'the fractal analyses is probably valid because of the large length-scales and small flame stretch rates, unlike turbulent flames in many engineering applications where the flame stretch rate usually reduces the burning rate' [3]. This is in line with the analysis of 20 unconfined explosions carried out earlier by Gostintsev *et al* [14]. They described the behaviour of spherical turbulent premixed flames propagation as a self-similar process in which a total flame front surface area grows $R^{1/3}$ times faster (theoretical fractal dimension $D = 2.33$) than the surface of a sphere with the same radius. According to the fractal theory a ratio of the turbulent flame front area A_t to the area of the smooth laminar spherical flame A_{u0} is equal to $A_t/A_{u0} = S_t/S_u = (\lambda_i/\lambda_0)^{(2-D)}$ [15], where S_u is laminar and S_t is turbulent burning velocities, respectively. Bearing in mind, that for freely propagating flames, the outer cut-off λ_0 is growing proportionally to the flame front radius R and the inner cut-off λ_i is a constant, the turbulent burning velocity S_t is a function of the average flame front radius R : $S_t/S_{t0} = (R/R_0)^{(D-2)}$, where S_{t0} is the burning velocity at radius R_0. It was reported [14] that for stoichiometric hydrogen–air mixtures a self-similar regime of flame propagation is established at a critical radius of 1.0–1.2 m. Different values have been proposed for the fractal dimension, D. Gouldin [15] used $D = 2.37$ adopted from [16]. A wide range of experimental values of fractal dimension $D =$ 2.11–2.36 was cited for premixed combustion by Gulder in 1990 [17]. In 1999 [3] Bradley suggested a theoretical value $D = 2.33$ for freely propagating flames. Gostintsev *et al* [18] demonstrated in 1999 that for self-similar freely propagating flames the fractal dimension is within the range $D = 2.2$–2.33. In 2000 Gulder reported, for turbulent premixed combustion in Bunsen-type burners, the fractal dimension within the range $D = 2.14$–2.24 [19].

This study is devoted to LES modelling and validation of the model, with two combustion sub-models, one based on the renormalization group (RNG) theory and another on the fractal theory, against the largest ever performed experiment on stoichiometric hydrogen–air deflagration in the open atmosphere GHT 34 [2]. In this paper simulation results are compared against experimental data on flame propagation, flame shape and overpressure transients at different distances from ignition source. The value of fractal dimension for use in LES of large-scale explosions is determined. More information relevant to this study could be found in [20–33].

2. Largest hydrogen–air deflagration test in atmosphere

A series of experiments with near stoichiometric hydrogen–air deflagrations, in unconfined hemispherical volumes, was performed in 1983 by the Fraunhofer Institute for Propellants and Explosives [2]. The experimental conditions and main results are presented in table 1. The principal aim of these experiments was to investigate the dependence of flame propagation velocity on the cloud size. Mixtures were ignited on the ground level inside the shell made of thin polyethylene (PE) film to exclude the effect of reflected pressure waves.

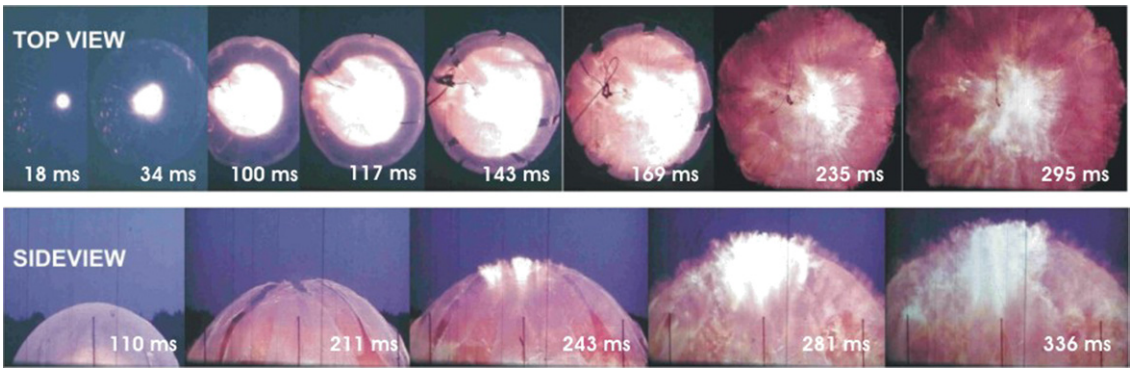

Figure 1. Snapshots of test GHT 34 in a 20 m diameter hemisphere.

Burnout of the cloud occurs approximately at two initial diameters corresponding to the cubic root of the products expansion coefficient. After burnout the peak overpressure decays with distance from the initiation point. The duration of the positive and the negative phases is independent of the distance for any given size of balloon. The amplitude of negative pressure peak was usually somewhat larger than that of the positive pressure phase and the negative phase being of shorter duration. For spherical sonic waves the authors [2] cited a theoretical result obtained by Landau that at any distance the integral of overpressure in time should be equal to zero. This theoretical result complies with experimental records of the outward propagating pressure wave outside the combustion area (see pressure transients at 35 and 80 m below). Processing of visual images of the flame propagation yielded a continuous increase in flame propagation velocity up to a maximum value, which was reached at a distance between the initial radius of the cloud R_{hsph} and 1.5 R_{hsph}. For initially quiescent stoichiometric hydrogen–air mixture this upper limit was estimated as 125 m s^{-1} with a peak overpressure 13 kPa assuming the validity of the authors' approach [2] based on simple turbulent combustion models of Damkohler and Karlovitz. The experimental results indicate that the flame propagation velocity approaches an upper limit with an increase in the cloud size.

In test GHT 34, with hydrogen–air mixture 29.7% by volume in a 20 m diameter hemisphere, the maximum flame propagation velocity was 84 m s^{-1} with the initial burning velocity estimated by authors [2] as 2.39 m s^{-1} (the expansion coefficient of combustion products was calculated as 7.26 with a density of combustible mixture 0.8775 kg m^{-3} and a speed of sound 397.3 m s^{-1}). Errors in velocity measurements were assessed as +5% without taking into account certain asymmetries in flame propagation. In the 2094 m^3 hemisphere experiment, GHT 34, a rhombus-shaped wire net was laid over the hemispherical balloon which was fastened to the ground at 16 points to compensate the buoyancy force. In order to make the hydrogen–air flame visible in daylight finely ground NaCl powder was dispersed inside the balloon at the end of the filling process to produce a yellow-coloured flame. Generally 10 to 12 piezo-resistive Kistler pressure sensors (100 kPa range, natural frequency 14 kHz) were used. These were mounted in a steel case having a mass of 20 kg in a way that their pressure-sensitive surfaces were fitted flush with the surface of the ground and covered with a 2 mm thick layer of silicone grease on the membrane to avoid the influence of temperature and heat radiation. In addition a sensor, located at a 5 m distance from the ignition source, was protected by means of a laminated plastic plate screwed to the steel casing and having an opening of 4 mm diameter in the middle. For the GHT 34 test an additional pressure sensor was installed at right angles to the axis with main sensors and mounted on a vertical timber wall 1 × 1 m^2 (head-on measurement). The explosion pressure was measured at distances 2.0, 3.5, 5.0, 6.5, 8.0, 18, 25, 35, 60 and 80 m from the initiation point. The mixture was ignited by pyrotechnical charges with total ignition energy 150 J. The pressure transients of sensors inside the combustion products did not return to zero after the negative pressure phase, except for the sensor installed at 5 m. This can be attributed to the fact that the transducers were thermalized to high temperatures during the explosion. Since they did not remain at the temperature at which they were calibrated, they were no longer calibrated and did not return to the baseline. This is an indication that the protective measures taken by the experimenters to insulate these transducers were insufficient for this large test.

Experimental results for flame propagation and pressure dynamics for test GHT 34 are presented in figures 4 and 6 and discussed further in the paper. The flame propagated in an almost hemispherical form. The balloon shell first stretched slightly outwards until it burst when the flame had reached about half of the original radius of the balloon 0.5R_0 (figure 1).

The explosion overpressure of about 6 kPa was practically the same within the cloud distances in GHT 34 test. A sharp overpressure peak Δp_F of about 10 kPa in the pressure transients followed flame propagation. This peak occurs when the flame passes the sensor on the ground. The cause for the occurrance of this peak is not clear, but is probably associated with the mounting of the PE foil in the sensor housing.

3. The LES model description

3.1. Governing equations

The main governing equations of the LES model were described elsewhere [34–36]. The equations were obtained by the filtering (filter size is CV size) of three-dimensional conservation equations for mass, momentum, energy, progress

variable and air concentration for compressible Newtonian fluid:

$$\frac{\partial \bar{\rho}}{\partial t} + \frac{\partial}{\partial x_j}(\bar{\rho}\tilde{u}_j) = 0, \tag{1}$$

$$\frac{\partial \bar{\rho}\tilde{u}_i}{\partial t} + \frac{\partial}{\partial x_j}(\bar{\rho}\tilde{u}_j\tilde{u}_i) = -\frac{\partial \bar{p}}{\partial x_i} + \frac{\partial}{\partial x_j} \times \left(\mu_{\text{eff}}\left(\frac{\partial \tilde{u}_i}{\partial x_j} + \frac{\partial \tilde{u}_j}{\partial x_i} - \frac{2}{3}\frac{\partial \tilde{u}_k}{\partial x_k}\delta_{ij}\right)\right) + \bar{\rho} g_i, \tag{2}$$

$$\frac{\partial}{\partial t}(\bar{\rho}\tilde{E}) + \frac{\partial}{\partial x_j}(\tilde{u}_j(\bar{\rho}\tilde{E} + \bar{p})) = \frac{\partial}{\partial x_j}\left(\frac{\mu_{\text{eff}} c_p}{Pr_{\text{eff}}}\frac{\partial \tilde{T}}{\partial x_j} - \sum_m \tilde{h}_m\left(-\frac{\mu_{\text{eff}}}{Sc_{\text{eff}}}\frac{\partial \tilde{Y}_m}{\partial x_j}\right) + \tilde{u}_i\mu_{\text{eff}}\left(\frac{\partial \tilde{u}_i}{\partial x_j} + \frac{\partial \tilde{u}_j}{\partial x_i} - \frac{2}{3}\frac{\partial \tilde{u}_k}{\partial x_k}\delta_{ij}\right)\right) + \bar{S}_E, \tag{3}$$

$$\frac{\partial}{\partial t}(\bar{\rho}\tilde{c}) + \frac{\partial}{\partial x_j}(\bar{\rho}\tilde{u}_j\tilde{c}) = \frac{\partial}{\partial x_j}\left(\frac{\mu_{\text{eff}}}{Sc_{\text{eff}}}\frac{\partial \tilde{c}}{\partial x_j}\right) + \bar{S}_c, \tag{4}$$

$$\frac{\partial}{\partial t}(\bar{\rho}\tilde{Y}_a) + \frac{\partial}{\partial x_j}(\bar{\rho}\tilde{u}_j\tilde{Y}_a) = \frac{\partial}{\partial x_j}\left(\frac{\mu_{\text{eff}}}{Sc_{\text{eff}}}\frac{\partial \tilde{Y}_a}{\partial x_j}\right) - \frac{Y_a}{Y_f + Y_a}\bar{S}_c. \tag{5}$$

The model is of the numerical type, as defined by Pope for a case of equivalence between filter and cell size, and does not include an 'artificial, i.e. non-physical, parameter Δ' [37] applied in some LES models in a source term of the progress variable equation.

The RNG turbulence model by Yakhot *et al* [38] was employed to model sub-grid scale (SGS) turbulence. In this model the effective viscosity is equal to $\mu_{\text{eff}} = \mu[1 + H(\mu_s^2\mu_{\text{eff}}/\mu^3 - 100)]^{1/3}$, where $\mu_s = \bar{\rho}(0.157V_{CV}^{1/3})^2\sqrt{2\tilde{S}_{ij}\tilde{S}_{ij}}$, $H(x)$ is the Heaviside function and the rate of strain tensor is $\tilde{S}_{ij} = 1/2((\partial\tilde{u}_i/\partial x_j) + (\partial\tilde{u}_j/\partial x_i))$. The RNG model is similar to the Smagorinsky's model [39], but does not contain adjustable or ad hoc parameters and is capable to describe transitional and laminar flow regimes: in the laminar flow the Heaviside function argument is negative and the effective viscosity recovers molecular viscosity, $\mu_{\text{eff}} = \mu$. In present simulations the values of molecular Prandtl and Schmidt numbers were chosen equal to those characteristic for air: $Pr = 0.7$, $Sc = 0.7$. The effective Prandtl number was calculated according to the RNG theory [38] for non-reactive flows and was equal to the effective Schmidt number:

$$\left|\frac{1/Pr_{\text{eff}} - 1.3929}{1/Pr - 1.3929}\right|^{0.6321}\left|\frac{1/Pr_{\text{eff}} + 2.3929}{1/Pr + 2.3929}\right|^{0.3679} = \frac{\mu}{\mu_{\text{eff}}}.$$

The conservation equation for air concentration (5) is introduced into the model to account for dilution of initial stoichiometric hydrogen–air cloud with ambient air.

3.2. The combustion model

The combustion model is based on the equation for the progress variable (4) and the gradient method. The source term in the energy equation (3) is a heat release rate due to combustion, $S_E = H_c \cdot S_c$. The mass burning rate is modelled similar to [34–36] using the gradient method $\bar{S}_c = \rho_u \cdot S_t \cdot |\nabla\tilde{c}|$. The gradient method allows decoupling between the physical requirement to keep the turbulent mass burning rate equal to $\rho_u S_t$ and a numerical requirement for a simulated flame front to occupy 4–5 CVs, when the gradient method is applied, independent of a mesh size and a scale of a problem. However, the integral of the source term throughout a numerical flame front thickness always gives a physically correct value for the mass burning rate per unit area, i.e. $\rho_u S_t$, independent of the numerical flame front thickness. As a result, simulations (flame propagation and pressure dynamics) will not be affected noticeably, regardless of the fact that the structure and size of a numerical flame front are not actual characteristics of the prototype. Furthermore, by tackling real problems with a scale of tens and hundreds of metres, there is no chance of resolving a whole structure of real turbulent flame front, where the turbulence generated by the flame front itself plays a role at scales comparable to the thickness of real flamelets of the order of millimetre. Nevertheless, the giving up of a fine flame front structure resolution allows one to reproduce reasonably hydrodynamics of flows ahead and behind the numerical flame front, overall flame propagation and explosion pressure dynamics because energy release in a flame front is kept physically correct.

The following general form for dependence of burning velocity on hydrogen concentration, Y_{H_2}, temperature, T, and pressure, p, is a general feature of the model (in the approximation of adiabatic compression/expansion $\varepsilon = m_0 + n_0 - m_0/\gamma_u$):

$$S_u(Y_{H_2}, T, p) = S_{u0}(Y_{H_2}) \cdot \left(\frac{T}{T_{u0}}\right)^{m_0(Y_{H_2})}\left(\frac{p}{p_0}\right)^{n_0(Y_{H_2})} = S_{u0}(Y_{H_2}) \cdot (p/p_0)^{\varepsilon(Y_{H_2})}. \tag{6}$$

This equation is a convenient and widely used approximation of the theoretical formula for burning velocity $S_u \propto k \cdot p^{n_0} \cdot \exp(-E_{\text{act}}/2R_{\text{univ}}T_b)$, where k is the pre-exponential factor, in a comparatively narrow range of temperatures between the temperature of combustion products at initial conditions, T_{bi}, and at the end of combustion, T_{be}. It was demonstrated that an error of the approximation does not exceed 15% [40].

The dependence of burning velocity on hydrogen concentration was accounted for by using a linear function $f(Y_{H_2})$, equal to 1 in the stoichiometric mixture (29.7% by volume of hydrogen) and 0 at the lower flammability limit (4% by volume of hydrogen): $S_{u0}(Y_{H_2}) = S_{u0}^{\text{Stoich}} \cdot f(Y_{H_2})$.

Two combustion sub-models applied in this study, i.e. the RNG combustion sub-model and the fractal combustion sub-model, are described below. For both models a common component, giving some augmentation to flame propagation velocity in simulations, is partially resolved flame front wrinkling due to hydrodynamic instability. The initial value of global (stretched) laminar burning velocity $S_{u0} = 1.91\,\text{m s}^{-1}$, obtained by Lamoureux *et al* [41] through direct registration of flame propagation by a schlieren system and a high speed camera system, was applied in this study in equation (6) for 29.7% hydrogen–air mixture.

3.2.1. RNG combustion sub-model. The first model applied to model turbulent burning velocity S_t is based on the RNG premixed turbulent combustion model [42] and the theoretical analysis of self-turbulized flames by Karlovitz *et al* [43].

Based on the analysis by Karlovits *et al* [43] the maximum value of the flame wrinkling factor due to the turbulence generated by flame front itself can be estimated as $\Xi_{MAX} = (E_i - 1)/\sqrt{3}$. For stoichiometric hydrogen–air mixture it gives the value $\Xi_{MAX} = 3.6$. The following dependence of the SGS flame wrinkling factor on flame front radius was assumed in this study to model a smooth increase in flame front surface area during transition from laminar to fully developed turbulent flame:

$$\Xi_{SGS}(R) = 1 + (\Xi_{MAX} - 1)(1 - \exp(-R/R_0)), \qquad (7)$$

where R_0 is a characteristic radius at which transition to the self-turbulized regime takes place. Gostintsev *et al* [14] reported previously that the characteristic radius for the onset of a self-similar regime of flame propagation for stoichiometric hydrogen–air mixture is $R_0 = 1.0 - 1.2$ m and the value $R_0 = 1.2$ m was adopted here.

The joint effect of 'large-scale' flow turbulence and SGS 'small-scale' turbulence generated by the flame front itself on the turbulent burning velocity was accounted for through the implementation of Yakhot's formula for premixed turbulent combustion, based on the RNG analysis [42], into the LES model in the following form:

$$S_t = [S_u \cdot \Xi_{SGS}(R)] \cdot \exp(u'/S_t)^2. \qquad (8)$$

The difference with the original Yakhot's formula is the use of SGS turbulent burning velocity $[S_u \cdot \Xi_{SGS}(R)]$ in our study instead of laminar burning velocity S_u. This is to account for a physical phenomenon of turbulence generated by flame front itself, acting at SGS, in the LES model.

3.2.2. Fractal combustion sub-model. The second combustion sub-model, applied to simulate the open atmosphere hydrogen–air explosion, is based on the fractal analysis of the freely propagating premixed flames and was described previously [44]. Following the conclusions of the fractal theory the burning velocity is modelled as

$$S_t = S_t^{R_0} \cdot f(Y_{H_2}) \cdot (R/R_0)^{D-2}, \qquad (9)$$

where $S_t^{R_0}$ is the burning velocity at radius R_0 of the onset of self-similar (fractal) regime of flame propagation and D is a fractal dimension. The theoretical value $D = 2.33$ corresponds to the upper limit of the experimentally observed range $D = 2.20$–2.33 reported by Gostintsev *et al* [28] for freely propagating flames in the open atmosphere.

Self-similar (fractal) regime of flame propagation takes place at flame radii above critical $R > R_0$. Hence, the fractal combustion sub-model can be applied only after that. The simulations of the transitional stage of the deflagration (flame radius $R < R_0$) were performed by the RNG sub-model. The value of burning velocity, extracted from the RNG sub-model at $R = R_0$ for implementation in formula (9) of the fractal sub-model, was calculated as $S_t^{R_0} = 6.44\,\mathrm{m\,s^{-1}}$ by the following procedure. The location of a simulated flame front, at any moment of time, was determined by the averaging of coordinates of all CVs with values of the progress variable within the range $c = 0.01$–0.99. At the moment when the radius of the flame front became equal to R_0 a total mass burning rate in the flame front was calculated. Then, to obtain the sought burning velocity, the mass burning rate was divided by the product of a combustible mixture density and the area of the hemisphere with radius R_0. The obtained value $S_t^{R_0} = 6.44\,\mathrm{m\,s^{-1}}$ is $\Xi = 6.44/1.91 = 3.37$ larger compared with the laminar burning velocity for the hydrogen–air mixture 29.7% by volume. This augmentation of burning velocity is due to the effects of turbulence generated by flame front itself and flow turbulence. The augmentation of burning velocity for radii $R > R_0$ was calculated in the fractal sub-model by equation (9) in place of equations (7) and (8) in the RNG sub-model.

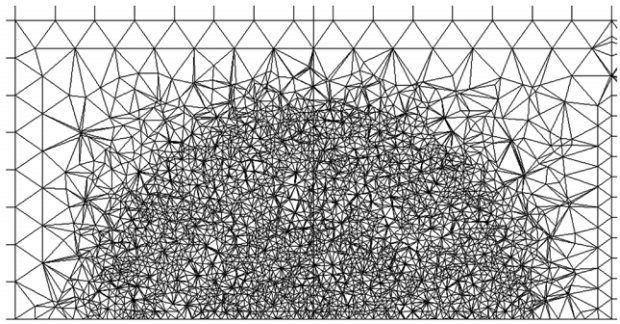

Figure 2. Cross section of the central part of the calculation domain.

3.3. Numerical details

3.3.1. Initial and boundary conditions. Initial temperature and initial pressure were equal to 283 K and 98.9 kPa, respectively, as in the experiment. Mixture was quiescent at ignition, $u = 0$. The progress variable was equal to $c = 0$ all over the domain. Air concentration was equal to $Y_a = 0.9713$ within the hydrogen–air cloud ($R \leqslant R_{hsph}$) and $Y_a = 1.0$ beyond it ($R > R_{hsph}$).

The no-slip impermeable adiabatic boundary condition was used on the ground. Non-reflecting boundary conditions were used on the boundaries representing the far-field in the atmosphere.

Ignition was modelled by the increase in the progress variable from $c = 0$ to $c = 1$ in one CV during the period $t = 22$ ms calculated as a time of flame propagation through spherical CV equal by volume to the ignition tetrahedral CV. The value $c = 1$ was kept in the ignition CV until the moment 29 ms. No adjustment of simulation results in time was required with this procedure.

3.3.2. Calculation domain. The calculation domain with sides L × W × H = 200 × 200 × 100 m was created to simulate both the flame front and the pressure wave propagation. The characteristic size of the tetrahedral CVs in the flame propagation area ($R \leqslant 22$ m) was about 1 m and the characteristic size of the hexahedral CVs in the rest of the domain ($R \geqslant 30$ m) was 4 m. The transitional area ($22 < R < 30$ m) was meshed using a tetrahedral mesh with the CV size changing from 1 to 4 m. The total number of CVs was 294296. The cross section of the central part of the calculation domain ($0 < R < 30$ m) is shown in figure 2.

The grid sensitivity analysis was conducted for the RNG combustion sub-model, as a part of a standard benchmark

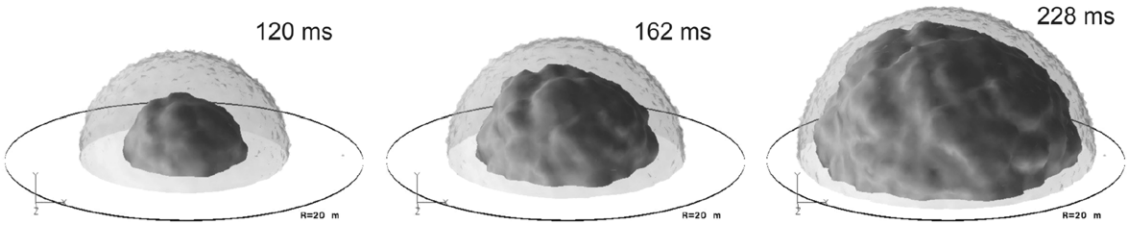

Figure 3. Snapshots of numerical simulation of flame front propagation in test GHT 34 (dark grey—flame front iso-surface $c = 0.5$, light grey—unburnt hydrogen–air mixture).

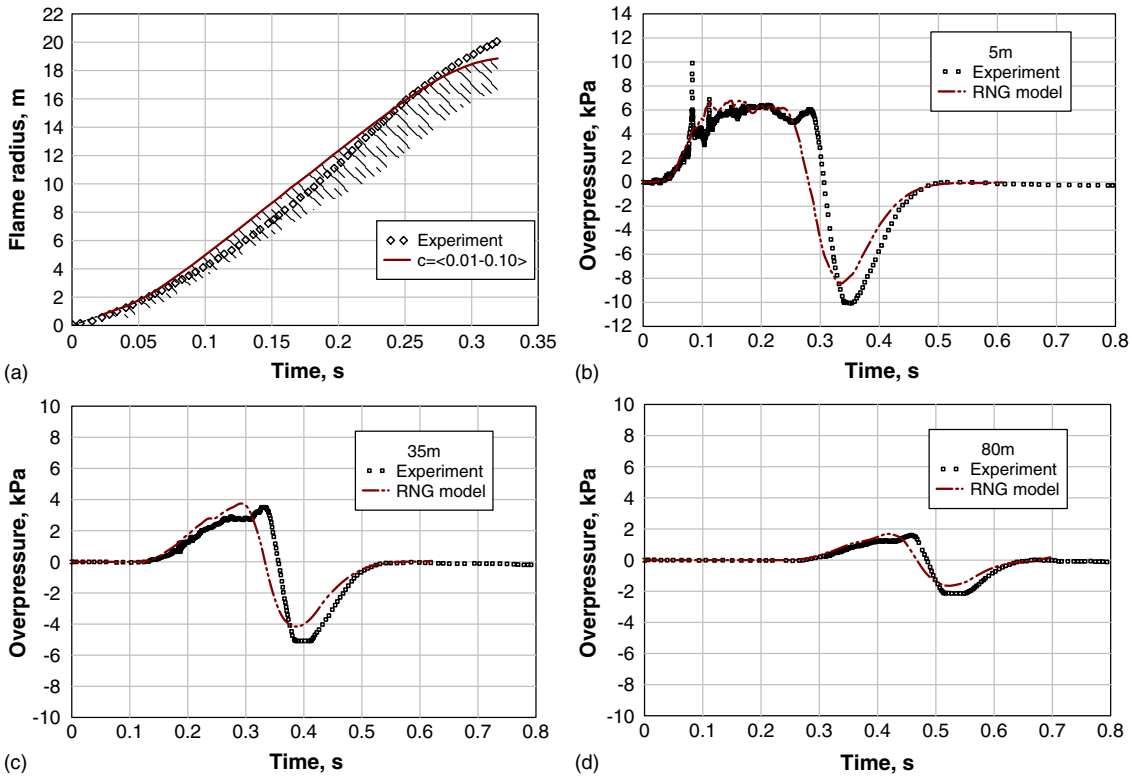

Figure 4. Comparison between experiment and simulations by the RNG combustion sub-model: (*a*) flame front propagation dynamics: solid line—leading flame edge (averaging through CVs with the progress variable within the range 0.01–0.10), hatched area—numerical flame front thickness; (*b*)–(*d*) pressure dynamics at $R = 5$ m, $R = 35$ m and $R = 80$ m, respectively.

exercise in the framework of activities of the European Network of Excellence HySafe [45]. Two similar grids with a characteristic CV size in the area of flame propagation 1.0 m and 0.5 m, respectively, were used. The difference in the flame front propagation dynamics, i.e. the growth of the flame front radius in time, was about 5%. This difference is due to better resolution of the flame front wrinkling by the hydrodynamic instability for a finer grid, which provides a larger mass burning rate and, thus, faster flame propagation.

3.3.3. CFD solver and numerical scheme. The FLUENT 6.2.16 solver was employed as a platform for the realization of the LES model. The double precision parallel version of solver was used with explicit linearization of the governing equations. The second order upwind scheme was used for convection terms and the central difference scheme for diffusion terms. The 4-stage Runge–Kutta scheme was applied for time stepping. The Courant–Friedrichs–Lewy number was equal to $CFL = 0.8$ to ensure stability. Simulation of real time of deflagration and pressure wave propagation up to 0.63 s takes about 6 days on a workstation IBM630 (12GB RAM, 2CPUx1.2GHz Power 4, 1CPU SPECfp=961).

4. Simulation results

4.1. Flame shape

The simulated flame front propagation for experiment GHT 34 is shown in figure 3. Distinctive large-scale wrinkling of the flame front by the hydrodynamic instability can be seen. The cascade of characteristic wrinkles above a LES filter size, i.e. a cell size in the numerical LES approach, of 1 m is close in size to the experimentally observed [2] wrinkles as presented in our paper [46], where the simulated flame front profiles are compared against experimental data.

4.2. Flame front propagation and pressure dynamics

Figures 4–6 show a comparison between the experimental results of test GHT 34 and the numerical simulations for the two applied combustion sub-models.

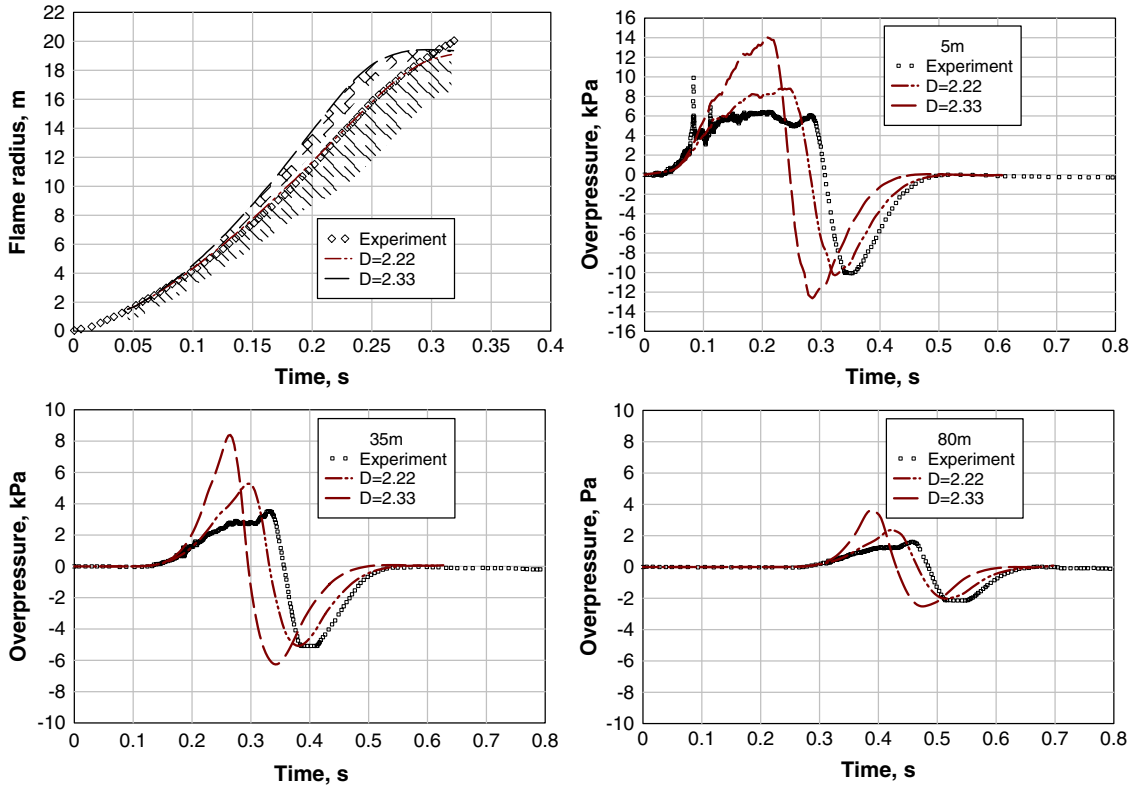

Figure 5. Comparison between experiment and simulations by the fractal combustion sub-model with fractal dimensions $D = 2.22$ and 2.33: (*a*) flame front propagation dynamics: lines—leading flame edge (averaging through CVs with the progress variable within the range 0.01–0.10), hatched area—numerical flame front thickness (only partially reproduced for $D = 2.33$); (*b*)–(*d*) pressure dynamics at $R = 5$ m, $R = 35$ m and $R = 80$ m, respectively.

Experimental data on flame propagation dynamics are represented in figures 4 and 5 as a change in the time position of a leading flame front edge. The thickness of a simulated flame front is shown in figure 4(*a*) by the hatched area with the leading flame edge depicted by a solid line. At final stages of deflagration the thickness of the numerical flame front is about 4 m which is close to experimental observations [46].

Both combustion sub-models reproduce the deceleration of flame at the final stage of the explosion, when the initial hydrogen–air mixture is diluted by atmospheric air that leads to a decrease in the burning rate (figure 5(*a*)). The deceleration of the numerical flame front is more pronounced compared with the experiment. This could be attributed to noticeably large cell sizes used in the simulations in the areas of mixture non-uniformity. Performing simulation on an adaptive grid in the area of large hydrogen concentration gradients could improve predictive capability of the model at final stages of deflagration. Some insignificant change in rear flame front edge dynamics can be seen in figure 4(*a*) at radius 10 m. This is apparently due to the numerical grid structure as the grid was generated having a sphere at radius 10 m in the calculation domain to separate the combustible mixture area from the ambient air area.

For the RNG combustion sub-model the maximum deviation of the simulated from the experimental leading flame front edge does not exceed 1 m. With this obviously good correlation between LES and experiment, the acceleration of the real flame front is reproduced only in the initial stage of the deflagration. At later stages simulations give practically constant flame propagation velocity (figure 4(*a*)). The simulated pressure dynamics (figures 4(*b*)–(*d*)) is close to experimental pressure transients at locations of properly functioning transducers at 5, 35 and 80 m. Both positive and negative phases of the pressure wave are reproduced by the numerical experiment, including arrival time, duration and decay of the pressure wave with distance. The amplitude of the positive phase of the pressure wave is reproduced in simulations exactly with a bit faster arrival time in a far-field. However, amplitude of the negative phase is up to 30% less than in experiment. The simulated rear front of the positive phase overpressure wave passes ahead of the experimental one due to significantly stronger deceleration of the flame front in simulation at the end of the deflagration compared with experiment.

Simulation results of the flame front propagation for two fractal dimensions, i.e. $D = 2.33$ and $D = 2.22$, are presented in figure 5(*a*). As expected the fractal sub-model simulations reproduce the monotonic increase in flame propagation velocity similarly to the experimental study [2]. Overpressure dynamics for both fractal dimensions are shown in figures 5(*b*)–(*d*). The simulation with theoretical fractal dimension $D = 2.33$ obviously over-predicts both flame propagation and overpressure dynamics. During numerical experiments it was found that a best fit value for the flame propagation dynamics for the fractal sub-model is $D = 2.22$, which is within the range $D = 2.20$–2.33 reported by Gostintsev *et al* [14]. One of the reasons for the optimum fractal dimension to be below the theoretical value is partial resolution of the flame wrinkling structure by LES. Indeed, it

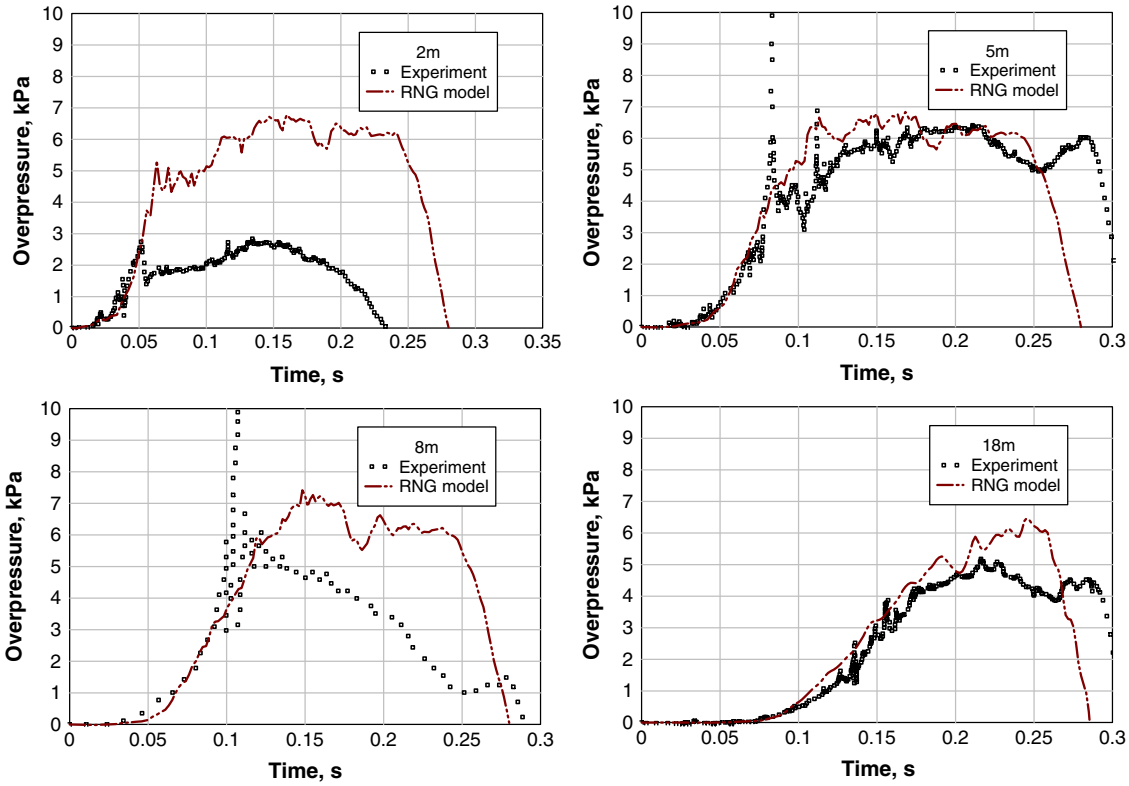

Figure 6. Comparison between experiment and simulation by the RGG combustion sub-model for pressure transients at the positive phase of the explosion pressure wave at locations 2 (*a*), 5 (*b*), 8 (*c*) and 18 m (*d*) from the ignition source.

was reported previously that for spherical flames the resolved fractal dimension is within the range 2.02–2.15 [34]. Along with good agreement in the prediction of the amplitude of the negative phase of the pressure wave the fractal sub-model over-predicts the amplitude of the positive phase by up to 50%. The reason for over-prediction of the positive pressure peak by the fractal model is not clear. This could be due to the effect of the PE balloon on the pressure wave. Indeed, segments of a balloon could 'consume' part of the energy in the pressure wave in the test. The effect of PE balloon segments is weakened at later stages and as a result the negative phase amplitude could be less affected.

The positive phase of the pressure wave at transducer locations inside the combustion zone, i.e. 2, 5, 8 and 18 m, is shown in figure 6. Transducers located at 2, 8 and 18 m from the ignition source were affected by the combustion products as their pressure transients did not return back to atmospheric pressure after the explosion. Still, pressure readings from these transducers may be used for explosion analysis until the time of flame arrival. A distinctive overpressure peak Δp_F of about 10 kPa in the pressure transients followed flame propagation (see figures 6(*b*) and (*c*)). The simulations reproduced an overpressure peak at the moment when the flame front arrived at the location of a sensor. Experimental pressure peak appears somewhat earlier compared with simulation results. It is in agreement with experimental data [2] where it was reported that the flame proliferates along the pressure measurement axis much more rapidly than in other directions. The fact of higher Δp_F at 5 and 8 m transducers could be explained by the intensification of combustion after the balloon shell had burst when the flame reached about half of the original radius of the balloon $0.5R_0$ (see figure 1). This is in line with results on easy DDT in hydrogen–air mixtures during venting of deflagration.

5. Conclusions

The LES model of large-scale accidental combustion is advanced further and applied to simulate the dynamics of the largest unconfined hydrogen–air deflagration ever performed. Two combustion sub-models were applied to analyse experimental data, one derived from the RNG theory and another from the fractal theory. Both sub-models include a SGS model of a transition from laminar to self-similar turbulent regime of flame propagation, which is based on a theoretical consideration by Karlovitz *et al* of the maximum turbulence generated by flame front itself and the results by Gostintsev *et al* on a critical radius of 1.0–1.2 m for the transition for stoichiometric hydrogen–air mixture.

Both combustion sub-models were applied in the calculation domain 200 × 200 × 100 m on an unstructured tetrahedral grid with a moderate number of CVs less than 300 000. Grid sensitivity analysis demonstrated that the LES model predictions vary to less than 5% for two unstructured tetrahedral grids with a difference in the characteristic cell size of 2.

Formation and decay of the pressure wave are reproduced in simulations, including the experimental observation that a negative phase has a shorter duration and a higher amplitude compared with a positive phase.

There is a more pronounced deceleration of simulated flame front at the end of deflagration compared with

experiment. It is thought to be due to insufficient resolution of the grid and affects slightly the duration of the positive phase of the pressure wave. Simulations on the adaptive grid in the area of hydrogen concentration gradients would better reproduce experimental data.

In the RNG combustion sub-model the effect of flow turbulence on the turbulent burning velocity is taken into account by the implementation of Yakhot's formula for turbulent premixed flame propagation velocity, which does not include either adjustable parameters or empirical coefficients. The RNG sub-model simulations reproduce initial flame acceleration and after that give practically constant flame front propagation velocity. The RNG sub-model is closer to experimental results in prediction of the positive phase but under-predicts by up to 30% the negative phase amplitude.

The fractal combustion sub-model gives a best fit to experimental flame propagation dynamics with a fractal dimension $D = 2.22$, which is within the range 2.20–2.33 reported by Gostintsev *et al* for large-scale unconfined explosions. Simulation with $D = 2.22$ reproduces accurately the experimentally observed flame front acceleration during the whole process of deflagration, the negative phase of the explosion pressure wave and overestimates by up to 50% the positive phase. Higher pressure peak of the positive phase in simulation compared with experiment could be attributed to the effect of the PE balloon. Simulations with theoretical value $D = 2.33$ apparently over-predicts both flame propagation and pressure dynamics.

Numerical simulations partially resolve flame front wrinkling due to hydrodynamic instability. This contributes by a factor of the order of 1.1 to the flame propagation velocity. The flow turbulence in the RNG sub-model contributes by an additional factor of the order of 1.15 to the burning velocity. Fractals increase the flame surface area in the fractal sub-model by a factor of the order of $(R/1.2)^{0.22}$ depending on the flame front radius, e.g. 1.74 for a radius $R = 15$ m. The turbulence generated by flame front itself is the main contribution to the augmentation of the turbulent burning velocity and equals to 3.6 for stoichiometric hydrogen–air mixture.

Both sub-models reproduce experimental flame front propagation dynamics up to 40 m diameter and pressure dynamics up to 80 m, i.e. at scales characteristic for hydrogen safety engineering problems. The agreement between numerical simulations and experimental data demonstrates the merits of the developed LES model for large-scale accidental premixed combustion.

Acknowledgments

Authors acknowledge the support of this work by their institutions and by the Commission of the European Union (Contract No 502630 HySafe 'Safety of Hydrogen as an Energy Carrier', www.hysafe.org).

References

[1] Dorofeev S B 1995 Blast effects of confined and unconfined explosions *Proc. 20th Symp. (Int.) on Shock Waves (Pasadena, CA, USA, July 1995)* pp 77–86

[2] Fraunhofer-institut fur treib-und explosivstoffe 1983. ICT-Projektforschung 1983. Forschungsprogramm "Prozeßgasfreisetzung—Explosion in der Gasfabrik und Auswirkungen von Druckwellen auf das Containment". Ballonversuche zur Untersuchung der Deflagration von Wasserstoff/Luft-Gemischen (Abschlußbericht). Projektleiter: H.Pförtner, Bearbeiter: H.Schneider, Dezember 1983

[3] Bradley D 1999 *Phil. Trans. R. Soc. Lond.* A 3567–81

[4] Hawkes E R and Cant R S 2001 Implication of a flame surface density approach to large eddy simulation of premixed turbulent combustion *Combust. Flame* **126** 1617–29

[5] Poinsot T and Veynante D 2001 *Theoretical and Numerical Combustion* (Edwards: Philadelphia)

[6] Kaufmann A, Nicoud F and Poinsot T 2002 Flow forcing techniques for numerical simulation of combustion instabilities *Combust. Flame* **131** 371–85

[7] Strehlow R A and Baker W E 1976 The characterization and evaluation of accidental explosions *Prog. Energy Combust. Sci.* **2** 27–60

[8] Zeldovich Ya B, Barenblatt G I, Librovich V B and Makhviladze G M 1980 *Mathematical Theory of Combustion and Explosion* (Moscow: Nauka)

[9] Makeev V I, Gostintsev Yu A, Strogonov V V, Bokhon Yu A, Chrnushkin Yu N and Kulikov V N 1983 Combustion and detonation of hydrogen–air mixtures in free spaces *Combust., Explosion Shock Waves* **19** 16–18

[10] Pförtner H 1985 The effects of gas explosions in free and partially confined fuel/air mixtures *Propellants, Explosives, Pyrotech.* **10** 151–5

[11] Becker Th and Ebert F 1985 Vergleich zwischen experiment und theorie der explosion grosser, freier Gaswolken *Chem. Ing. Tech.* **57** 42–5

[12] Gorev V A 1982 Comparison of the air explosion waves from different sources *Combust., Explosion Shock Waves* **8** 77
Bystrov S A and Gorev V A 1982 Interaction of explosion waves from a spherical deflagration with an obstacle *Combust., Explosion Shock Waves* **20** 113–6

[13] Dorofeev S B, Sidorov V P and Dvoinishnikov A E 1995 Blast parameters from unconfined gaseous detonations *Proc. 20th Symp. (Int.) on Shock Waves (Pasadena, CA, USA, July 1995)* pp 673–8

[14] Gostintsev Yu A, Istratov A G and Shulenin Yu V 1988 Self-similar propagation of a free turbulent flame in mixed gas mixtures *Combust., Explosion Shock Waves* **24** 63–70

[15] Gouldin F C 1987 *Combust. Flame* **68** 249–66

[16] Abdel-Gayed R G, Al-Khishali K J and Bradley D 1984 *Proc. R. Soc. Lond.* A 391 393–414

[17] Gulder O L 1990 Turbulent premixed combustion modelling using fractal geometry *Proc. Comb. Inst.* **23** 835

[18] Gostintsev Yu A, Istratov A G, Kidin N I and Fortov V E 1999 *High Temp. Thermophys.* (Teplofizika Vysokih Temperatur) **37** 633–7 (in Russian)

[19] Gulder O L *et al* 2000 Flame front surface characteristics in turbulent premixed propane/air combustion *Combust. Flame* **120** 407–16

[20] Lee J H S 1977 Initiation of gaseous detonation *Ann. Rev. Phys. Chem.* **28** 75–104

[21] Bull D C and Martin J A 1977 Explosion of unconfined clouds of natural gas *American Gas Association, Transmission Conf.* (Missouri, USA 16–18 May)(*AGA Operating Section Proc.*) Paper 77-T-40

[22] Lee J H S and Moen I O 1980 The mechanism of transition from deflagration to detonation in vapor cloud explosions *Prog. Energy Combust. Sci.* **6** 359–89

[23] Moen I O, Lee J H S, Hjertager B H, Fuhre K and Eckhoff R K 1982 Pressure development due to turbulent flame propagation in large-scale methane-air explosions *Combust. Flame* **47** 31–52

[24] Pfortner H 1983 Flame acceleration and pressure build up in free and partially confined hydrogen-air clouds

9th Colloquium on the Dynamics of Explosions and Reactive Systems (Poitiers, France: ICDERS)
[25] Pfortner H 1985 The effects of gas explosions in free and partially confined fuel/air mixtures *Propellants, Explosives, Pyrotech.* **10** 151–5
[26] Pikaar M J 1985 Unconfined vapour cloud dispersion and combustion: an overview of theory and experiments *Chem. Eng. Res. Des.* **63** 75–81
[27] Berman M 1986 Critical review of recent large-scale experiments on hydrogen–air detonations *Nucl. Sci. Eng.* **93** 321–47
[28] Moen I O, Bjerketvedt D, Jenssen A and Thibault P A 1985 Transition to detonation in a large fuel–air cloud *Combust. Flame* **61** 285–91
[29] Leyer J C, Desbordes D, Saint-Cloud J P and Lannoy A 1993 Unconfined deflagrative explosion without turbulence: experiment and model *J. Hazard. Mater.* **34** 123–50
[30] Moen I O 1993 Transition to detonation in fuel–air explosive clouds *J. Hazard. Mater.* **33** 159–92
[31] Dorofeev S B, Sidorov V P and Dvoinishnikov A E 1996 Deflagration to detonation transition in large confined volume of lean–hydrogen–air mixtures *Combust. Flame* **104** 95–110
[32] Khokhlov A M, Oran E S, Wheeler J C 1997 A theory of deflagration-to-detonation transition in unconfined flames *Combust. Flame* **108** 503–17
[33] Kelly T J, Pierorazio A J, Goodrich M L, Kolbe M, Baker Q A and Ketchum D E 2003 Deflagration to detonation transition in unconfined vapor cloud explosions *18th Annual Int. Conf. - Managing Chemical Reactivity Hazards and High Energy Release Events, (Scottsdale (AZ), 23–25 September 2003)* (New York: Center for Chemical Process Safety) pp 155–68
[34] Molkov V, Makarov D and Grigorash A 2004 Cellular structure of explosion flames: modelling and large eddy simulation *Combust. Sci. Tech.* **176** 851–85
[35] Makarov D and Molkov V 2004 Large eddy simulation of gaseous explosion dynamics in an unvented vessel *Combust., Explosion Shock Waves* **40** 136–44
[36] Molkov V and Makarov D 2004 Large eddy simulation of hydrogen–air explosion at elevated temperature *Adv. Chem. Phys.* **23** 25–36
[37] Pope S B 2004 Ten questions concerning the large-eddy simulation of turbulent flows *New J. Phys.* **6** 1–24
[38] Yakhot V and Orszag S 1986 Renormalization group analysis of turbulence: I. Basic theory *J. Sci. Comput.* **1** 3–51
[39] Smagorinsky J 1963 General circulation experiments with the primitive equations: I. The basic experiment *Mon. Weather Rev.* **91** 99–164
[40] Babkin V S, Viun A V and Kozachenko L S 1966 The investigation of pressure dependence of burning velocity by the constant volume bomb method *Combust., Explosion Shock Waves* **2** 52–60
[41] Lamoureux N, Djebaili-Chaumeix N and Paillard C E 2002 Laminar flame velocity determination for H2-air-steam mixtures using the spherical bomb method *J. Phys. IV (France)* **12** Pr7-445–7-458
[42] Yakhot V 1988 Propagation velocity of premixed turbulent flames *Combust. Sci. Technol.* **60** 191–214
[43] Karlovitz B, Denniston D W Jr and Wells F E 1951 Investigation of turbulent flames *J. Chem. Phys.* **19** 541–7
[44] Makarov D, Molkov V and Gostintsev Yu 2006 Comparison between RNG and fractal combustion models for LES of unconfined explosions *Combust. Sci. Technol.* at press
[45] www.hysafe.org
[46] Molkov V V, Makarov D V, Schneider H 2006 Hydrogen-air deflagrations in open atmosphere: large eddy simulation analysis of experimental data *Int. J. Hydrog. Energy* submitted